Exchange-spring behavior in epitaxial hard/soft magnetic bilayers

Eric E. Fullerton,* J. S. Jiang, M. Grimsditch, C. H. Sowers, and S. D. Bader
Materials Science Division, Argonne National Laboratory, Argonne, Illinois 60439
(Received 9 June 1997)

We present results on the magnetic reversal process in epitaxial Sm-Co($1\bar{1}00$)/TM (TM=Fe,Co) bilayer films prepared via magnetron sputtering. The magnetically hard Sm-Co films have 20-T uniaxial anisotropy and coercivities >3 T at room temperature, that double on cooling, as determined by magnetometry. The TM layers are exchange coupled to the Sm-Co layer and exhibit reversible demagnetization curves expected for an exchange-spring magnet. We also present numerical solutions of a one-dimensional model that provide the spin configuration for each atomic layer. Comparison of the experimental results with the model simulations indicates that our exchange-spring behavior can be understood from the intrinsic parameters of the hard and soft layers. The simulations are extended to realistically estimate the ultimate gain in the energy product that potentially can be realized based on the exchange hardening principle. [S0163-1829(98)00742-5]

I. INTRODUCTION

Exchange-spring magnets are composed of a two-phase distribution of hard- and soft-magnetic grains that have potential applications as permanent magnets.[1] The hard-magnetic grains provide the high anisotropy and coercive fields while the soft-magnetic grains enhance the magnetic moment with the additional benefit of reducing the rare-earth content since the soft phase can be rare-earth free. The soft grains are pinned to the hard-magnet grains at the interfaces by the exchange interaction while the center of the soft-magnet grains can rotate in a reversed magnetic field. Such magnets are characterized by enhanced remanent magnetization and reversible demagnetization curves since the soft grains will rotate back into alignment with the hard grains when the applied field is removed. Although future application of two-phase magnets will most likely be based on randomly dispersed nanocomposite geometries,[2] coupled bilayer films provide convenient model systems for studying their properties because the relative length scales (i.e., thicknesses of the hard- and soft-magnet layers) can be controlled during the deposition process. Skomski[3] and Coey[2] explored the theory of exchange coupled films and predicted that a giant energy product of 120 MGOe (about three times that of commercially available permanent magnets) is possible in superlattice structures consisting of aligned hard-magnet layers that are exchange coupled to soft layers with high magnetization.

Realization of exchange-coupled thin-film structures requires controlled growth of nanometer-scale hard-magnet films. The growth of such films, their incorporation into suitable magnetic heterostructures, and understanding their magnetic reversal behavior are areas of current research.[4–10] In this paper we explore the reversal processes in epitaxial hard/soft Sm-Co(1100)/TM bilayers (TM=Fe and Co) with the transition-metal (TM) thicknesses in the range of 25–200 Å. Magnetically hard Sm-Co(1100) has the advantage of having a uniaxial in-plane anisotropy. Thus, the rotation process of the exchange-coupled TM layers can be studied with the applied field both parallel and perpendicular to the anisotropy axis of the hard layer.

The switching of a soft-magnet film coupled ferromagnetically to a hard layer was studied by Goto *et al.*[11] Under the assumption that the hard layer is perfectly rigid and the soft layer has no anisotropy, they solved for the magnetization of the soft layer with an applied field opposed to the hard layer. They found that the soft layer remains parallel to the hard layer for fields less than the exchange-bias field $H_{\rm ex}$, where $H_{\rm ex}$ is given by

$$H_{\rm ex}=\pi^2 A/2M_s t^2, \tag{1}$$

A is the exchange constant that couples spins within the soft layer, t is the soft layer thickness, and M_s is the saturation magnetization of the soft layer. For $H>H_{\rm ex}$, the spins in the soft layer exhibit continuous rotation, as in a Bloch wall, with the angle of rotation increasing with increasing distance from the hard layer. The magnetization of the soft layer is reversible and approaches saturation as $(H/H_{\rm ex})^{-0.5}$. Both predictions are consistent with experimental studies of NiFe/NiCo bilayers by Goto *et al.*, and with subsequent studies of Sm-Co/NiFe,[5] Sm-Co/Co-Zr,[6,7] and epitaxial $CoFe_2O_4/(MnZn)Fe_2O_4$ exchange-coupled bilayers.[8] In all these studies, the thickness of the soft layer was >500 Å. For sufficiently thin soft-magnetic layers ($t\sim$ a domain-wall width in the hard layer), the soft layer is expected to be rigidly coupled to the hard layer, with both layers switching at a nucleation field given by

$$H_N=\frac{2(t_h K_h+t_s K_s)}{t_h M_h+t_s M_s}, \tag{2}$$

where $t_h(t_s)$, $K_h(K_s)$, and $M_h(M_s)$ are the thickness, anisotropy, and magnetization of the hard (soft) layers, respectively. Such behavior has been shown qualitatively for Sm-Co/Fe-Co bilayers[9] and Nd-Fe-B/Fe superlattices.[10]

The present paper is organized as follows: we present experimental procedures in Sec. II, the magnetization of the Sm-Co films and Sm-Co/TM bilayers in Sec. III, compare the observed magnetic reversal behavior with numerical solutions of one-dimensional magnetic models of the system in Sec. IV, and summarize the major conclusions in Sec. V.

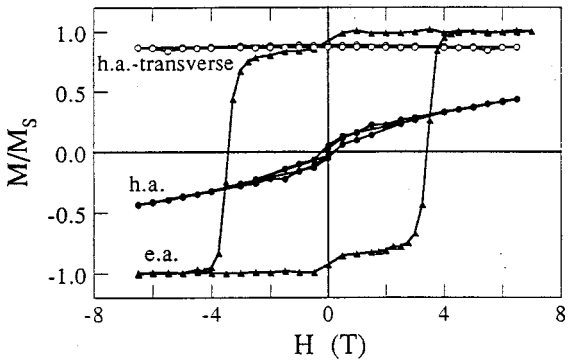

FIG. 1. Room-temperature magnetic hysteresis loops for a 200-Å Sm-Co(1100) film with H parallel to the hard-axis (h.a.) MgO[110] direction (circles) and the easy-axis (e.a.) [001] direction (triangles). For the hard-axis measurements, we show both the longitudinal (filled circles) and transverse (open circles) magnetization components.

II. EXPERIMENTAL PROCEDURES

The Sm-Co($\bar{1}100$)/TM bilayers are grown via dc magnetron sputtering onto single-crystal MgO(110) substrates coated with an epitaxial 200-Å Cr(211) buffer layer. The 200-Å Sm-Co layers are deposited by cosputtering from separate Sm and Co sources with a nominally Sm_2Co_7 concentration at a substrate temperature $T_s = 600\,^{\circ}C$ as outlined in Ref. 4. The TM layers are then grown at $T_s = 300-400\,^{\circ}C$ with thickness values of 25–200 Å and capped with a 50-Å Cr layer. The film structure was studied by x-ray diffraction. The magnetic properties were measured by means of (i) a Quantum Design 7-T superconducting quantum interference device magnetometer, (ii) the longitudinal magneto-optic Kerr effect (MOKE) using p-polarized, 633-nm light, and (iii) Brillouin light scattering (BLS). The BLS experiments were performed at room temperature using a 5-pass Fabry-Pérot interferometer and a single-mode argon laser operated at 514.5 nm. The magnetometer was equipped with coil sets to measure both the longitudinal and transverse magnetization. Because of the nonuniform rotation process expected in an exchange-spring magnet, the longitudinal and transverse data are not simply related (as they would for coherent rotation of a uniformly magnetized sample) and thus provide a more complete description of the magnetic reversal.

III. EXPERIMENTAL RESULTS

A. Sm-Co films

The structural and magnetic characterization of Sm-Co(1100) films grown onto Cr(211) buffer layers are described in detail in Refs. 12 and 13. The epitaxial relation for the Sm-Co(1100) films is Sm-Co[0001]‖Cr[011]‖MgO[001] resulting in a uniaxial in-plane structure with the magnetic easy axis parallel to the Sm-Co c axis. The nominal composition of the films is Sm_2Co_7. However, high-resolution electron microscopy identifies stacking disorder in the c-axis direction consisting of a mixture of $SmCo_3$, Sm_2Co_7, and $SmCo_5$ phases.[13] Shown in Fig. 1 are the magnetic hysteresis loops for a single 200-Å Sm-Co(1100) film measured with the field H applied along orthogonal in-plane directions. The films exhibit strong uniaxial in-plane anisotropy consistent with the expected c-axis anisotropy. For H parallel to the Sm-Co easy axis (MgO[001]), a square loop is observed with a coercive field H_c of 3.4 T for this film. The coercivity increases to 7.3 T at 25 K. The Sm-Co saturation magnetization is ~500–600 emu/cm^3 as compared to 1710 and 1425 emu/cm^3, for Fe and Co, respectively. For H applied in the orthogonal in-plane direction, a sheared hard-axis loop is measured. The anisotropy field, estimated from extrapolating the hard-axis loop to saturation, is ~20 T. This field value is comparable to those reported for bulk Sm_2Co_7 (>20 T) (Ref. 14) and $SmCo_5$ (25–44 T).[15]

Also shown in Fig. 1 is the transverse magnetization measured with H parallel to the hard axis. This measurement was obtained after the film was first saturated along the easy axis and then rotated 90° for the hard-axis measurements. For $H = 0$, the transverse moment equals the remanent easy-axis value. The moment decreases only ~5% from the remanent value in a field of 7 T along the hard axis indicating that the moments rotate <20° from the easy axis. The shoulder observed in the easy-axis magnetization near $H = 0$ may result from the presence of a minority soft magnetic phase. As will be seen later, however, such minority soft phases do not affect the switching of the TM layers.

B. Sm-Co/Fe bilayers

1. Magnetization

Shown in Fig. 2 are room-temperature hysteresis loops of the Sm-Co(200 Å)/Fe bilayers measured in the same geometry as Fig. 1. For a 25-Å Fe layer [Fig. 2(a)], the loop shapes are similar to those observed in Fig. 1. A square easy-axis loop is measured with a $H_c = 1.7$ T reduced ~50% as compared to the isolated Sm-Co film, indicating that the entire Fe layer is strongly coupled to the underlying Sm-Co film and that the two layers switch as a unit. The hard-axis transverse loop is reversible and decreases ~25% in a 7-T field resulting from the increased rotation of the Fe layer from the Sm-Co easy axis. For the 100- and 200-Å Fe layers the loops change shape quite significantly. For H applied parallel to the easy axis, separate switching transitions for the Fe and Sm-Co layers are observed. This is similar to that observed in Refs. 5–8 but with much thinner soft layers in the present samples. The switching fields for the Sm-Co layers (0.6–0.7 T) are similar for the 100- and 200-Å Fe layers and are only 20% of that of the isolated Sm-Co film value. The hard-axis data exhibit an initial low-field susceptibility that increases with increasing Fe layer thickness. The transverse magnetization also shows a rapid decrease at low fields. Both effects are due to the rotation of most of the Fe layer as H increases. This result is consistent with that observed for Sm-Co/Co-Zr films.[7]

2. Magneto-optic Kerr effect

Shown in Fig. 3 are the MOKE results for the 100- and 200-Å Fe layer films. As a result of the finite penetration of the light, the MOKE measurements are dominated by the switching of the top Fe layer. For the easy-axis measurement, the Fe layer starts to switch at the exchange field: 0.22 and 0.09 T for the 100- and 200-Å Fe layers, respectively. Above H_{ex}, a sharp drop in the magnetization is then fol-

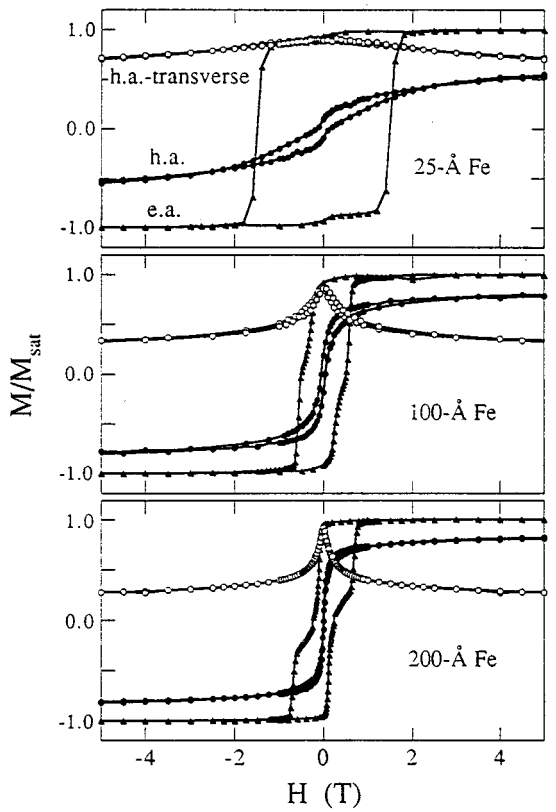

FIG. 2. Room-temperature magnetic hysteresis loops for Sm-Co/Fe bilayer films with H parallel to the hard-axis (circles) and the easy-axis (triangles) directions. For the hard-axis measurements, we show both the longitudinal (filled circles) and transverse (open circles) magnetization components.

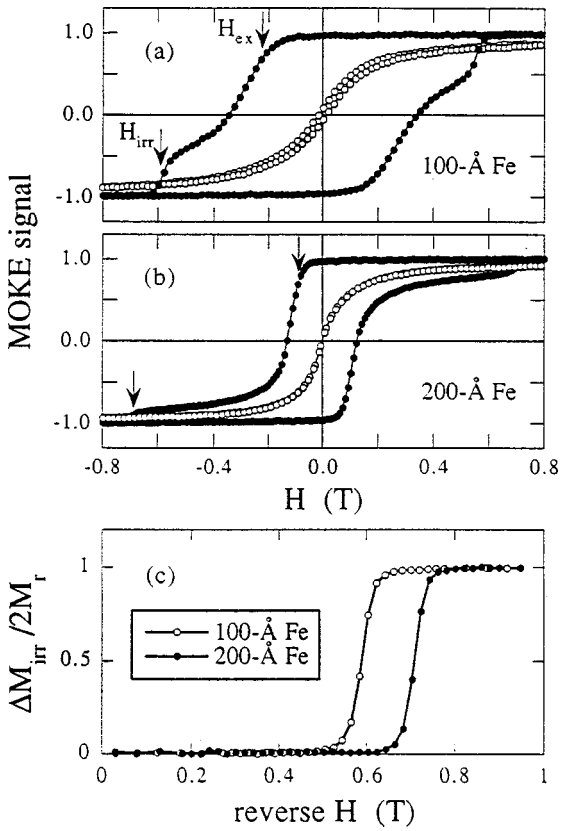

FIG. 3. Room-temperature magnetic properties of Sm-Co/Fe bilayer films measured by MOKE. Hysteresis loops measured with H parallel to the hard-axis (open circles) and the easy-axis (filled circles) directions for the 100-Å Fe (a) and 200-Å Fe (b) films. (c) The irreversible magnetization $\Delta M_{\rm irr}$ vs reverse field measured with H parallel to the easy axis, where $\Delta M_{\rm irr}$ is the difference between the remanence acquired after saturation in one direction and the remnant magnetization after subsequent application of a reverse field in the opposite direction.

lowed by an asymptotic approach to saturation until the hard layer switches irreversibly at $H_{\rm irr}$, as expected for the exchange-spring state. This behavior is particularly clear for the 200-Å Fe film. One characteristic of exchange-spring magnets is that the reorientation of the soft layer should be fully reversible for fields below the switching field of the hard layer. To test this behavior, we have measured the irreversible magnetization change as a function of field reversal for intermediate fields. Following Kneller and Hawig,[1] the irreversible magnetization is described by the field demagnetization remanence $M_d(H)$, the remanence being acquired after saturation in one direction and subsequent application of an applied field in the opposite direction. The irreversible magnetization change $\Delta M_{\rm irr}$ is given by $M_r - M_d(H)$ where M_r is the remanent magnetization. Shown in Fig. 3(b) is $\Delta M_{\rm irr}/2M_r$. The magnetization is fully reversible ($\Delta M_{\rm irr} = 0$) up to fields where the Sm-Co layer switches at $H_{\rm irr} = 0.6$ and 0.7 T for the 100- and 200-Å Fe layer films, respectively.

3. Brillouin light scattering

As a final probe of the magnetic properties we have examined the magnon frequencies of the Fe layers using BLS. Shown in Fig. 4 is the field dependence of the magnon frequency in the 100-Å Fe sample. As with MOKE, the BLS signal is dominated by contributions from magnons in the top Fe layer. The field is always parallel to the easy axis. The frequencies decrease with decreasing H, reaching a minimum at $H = -0.25$ T, and then increase for even lower fields. At $H \sim -0.55$ T, the frequency changes abruptly and becomes equal to the corresponding positive field value. Qualitatively these results are consistent with the magnetization studies:

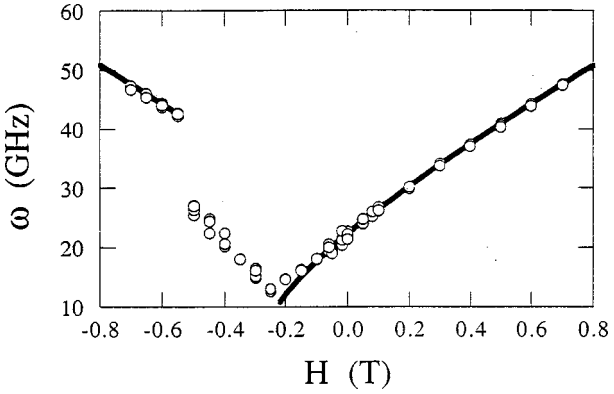

FIG. 4. Room-temperature BLS results for the Sm-Co/Fe(100 Å) bilayer film. The symbols are the magnon frequencies measured from saturation in positive fields towards negative fields. The solid line is a fit to Eq. (3).

the frequency minimum at ~ -0.25 T reflects the instability as the Fe layer starts to spiral away from the easy axis of the Sm-Co layer, and the jump at -0.55 T occurs as the Sm-Co layer switches.

We are not aware of any theory that quantitatively describes the magnon frequencies in a magnetic layer undergoing such a spiral reorientation. However, in the regions below -0.55 T and above -0.25 T, where the magnetization of the Fe layer lies along the easy axis of the SM-Co and is also either parallel or antiparallel to the applied field, the following quantitative analysis can be made. The magnon frequency for an isolated Fe film of thickness t (assuming no anisotropy) is given by[16]

$$\omega = \gamma[(H + 2\pi M_s)^2 - (2\pi M_s)^2 \exp(-2qt)]^{1/2}, \quad (3)$$

where $\gamma = 29.4$ GHz/T is the gyromagnetic ratio of Fe, and $q = 8.6 \times 10^{-4}$ Å^{-1} is the magnon wave vector determined by our scattering geometry. In order to use Eq. (3) for our samples it must be generalized to include the constraint of the Fe spins at the Sm-Co interface. Since the instability of the Fe magnetization occurs at $-H_{ex}$, it is reasonable to invoke H_{ex} as an effective exchange field. Replacing H by $H + H_{ex}$, Eq. (3) quantitatively fits the data in Fig. 4 and yields $H_{ex} = 0.22$ T (0.09 T for the 200-Å sample) and $4\pi M_s = 1.8$ T. The fit below $H = -0.55$ T is obtained in the calculation by considering the sign change of H_{ex} when the Sm-Co layer switches. The Brillouin scattering shows that the spin-wave frequencies of the Fe films are consistent with isolated Fe films perturbed by an effective exchange field. This demonstrates the model behavior of our system. A more rigorous description of the magnon modes that also describes the region in which the magnetization is in a spiral state will require solving the eigenmodes of the coupled-layered system, including the anisotropy of the Sm-Co layer, and satisfying the appropriate boundary condition at the interface, and is beyond the scope of this paper.

C. Sm-Co/Co bilayers

Shown in Fig. 5 are room-temperature hysteresis loops of the Sm-Co(200 Å)/Co bilayers. Square easy-axis loops are observed with coercive fields of 0.73 and 0.42 T for the 100- and 200-Å Co layers, respectively. The Sm-Co/Co results contrast with those on similar Sm-Co/Fe samples in important ways: (i) the Co layers remain parallel with the Sm-Co to well above the expected H_{ex} determined from Eq. (1), (ii) the Sm-Co and Co layers switch at the same field, and (iii) the switching field of the Sm-Co layer depends strongly on the Co layer thickness. The hard-axis loops are similar to those of the Sm-Co/Fe films, and exhibit an increased low-field susceptibility with increased Co layer thickness.

D. Low-temperature results

To further investigate the difference in switching of the Fe and Co layers, we examined the samples at low temperatures in order to increase the coercivity of the Sm-Co layers. For isolated Sm-Co films, the coercivity doubles on cooling from 300 to 25 K. Shown in Fig. 6 are easy-axis demagnetization curves for the 200-Å Co and Fe films measured at 25 K. Included in Fig. 6 are major loops as well as minor loops

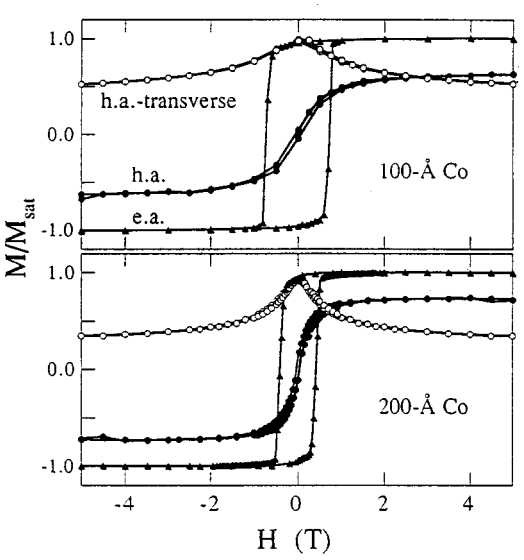

FIG. 5. Room-temperature magnetic hysteresis loops for Sm-Co/Co bilayer films with H parallel to the hard-axis (circles) and the easy-axis (triangles) directions. For the hard-axis measurements, we show both the longitudinal (filled circles) and transverse (open circles) magnetization components.

with the magnetization measured both longitudinal and transverse to the applied field. The Sm-Co/Fe results are similar to the room-temperature data with the exception that the switching of the Sm-Co layer has increased to 1.5 T but is still well below the ~ 7 T value for the Sm-Co film. The minor loop shows the switching of the Fe layer is completely reversible for field as large as 1.2 T confirming that the Fe and Sm-Co are strongly exchange coupled. For $H > H_{ex}$

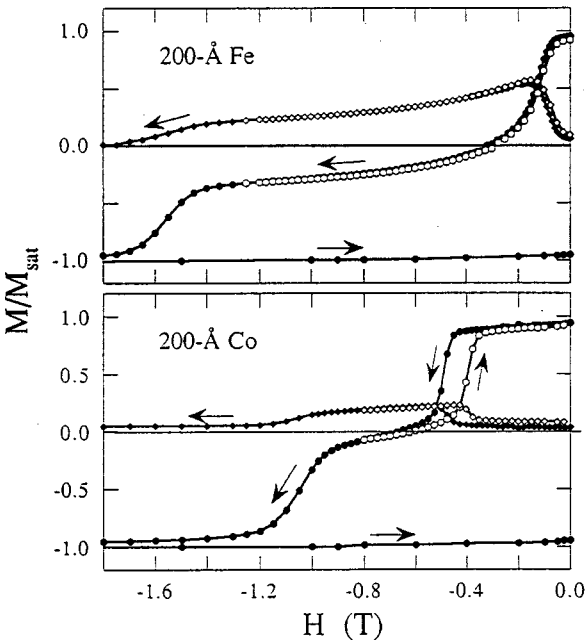

FIG. 6. Low-temperature (25 K) demagnetization curves for Sm-Co/Fe and Sm-Co/Co bilayer films with H parallel to the easy axis. We show both the longitudinal (circles) and transverse (diamonds) magnetization components. The filled symbols are the demagnetization curves and the open symbols are minor loops.

when the longitudinal moment decreases, the transverse moment first increases and then more slowly decreases with increasing field. In the exchange-spring state, the rotation of the spins away from the hard layer results in the significant transverse moment observed experimentally. The fact that such a large transverse moment is observed indicates that the Fe layer rotates with a preferred sense of rotation. This suggests that the applied field is slightly misaligned with the easy axis. If the field were perfectly aligned, then different regions of the samples would rotate with opposite sense of rotations and the net transverse magnetization would average to zero.

At 25 K, separate switching transitions are observed for the Sm-Co and Co layers at 1.05 and 0.5 T, respectively. The switching of the Co layer is reversible but is hysteretic about the exchange field $H_{ex}=0.46$ T ($H_{ex}=0.86$ T for the 100-Å Co samples). This behavior arises from the intrinsic magnetic anisotropy of the Co layer.[8] The *c*-axis Co anisotropy stabilizes the Co layer either parallel or antiparallel to the Sm-Co film and results in an abrupt and hysteretic behavior at the Co switching field. H_{ex} for the Co layer can be roughly estimated by assuming that at H_{ex} the Co layer rotates from being parallel to antiparallel with the Sm-Co layer. By equating the Zeeman energy gain with the energy of introducing a domain wall γ (~ 10 ergs/cm^2) in the Co layer near the interface, a rough estimate for H_{ex} is given by $\gamma/M_s t=0.36$ T, in reasonable agreement with the experimental results.

The observed low-temperature H_{ex} values for the Co layers are close to the room-temperature H_c values of the coupled bilayer. This suggests that the room-temperature H_c values for the Sm-Co/Co samples are determined primarily by H_{ex} of the Co layer. Once the Co layer switches the Sm-Co layer follows.

IV. SIMULATION

To obtain greater insight into the switching of both the soft and hard layers, we use the simple one-dimensional atomic model employed successfully in Refs. 5 and 7. We divide the bilayer structure into a sum of atomic layers and the bilayer is treated as a one-dimensional chain of spins normal to the layers. Each spin is characterized by a moment M_i, uniaxial anisotropy constant K_i, and is assumed to rotate within the plane of the film characterized by an in-plane angle θ_i. θ_i is measured relative to the easy-axis direction of the hard layer, and the external field is applied at an angle θ_H with respect to the easy axis. Adjacent spins are separated by $d=2$ Å and coupled by an exchange constant $A_{i,i+1}$. The total energy of the system is given by

$$E=-\sum_{i=1}^{N-1}\frac{A_{i,i+1}}{d^2}\cos(\theta_i-\theta_{i+1})-\sum_{i=1}^{N}K_i\cos^2(\theta_i)-\sum_{i=1}^{N}HM_i\cos(\theta_i-\theta_H). \tag{4}$$

For the bilayer system, the index $i=1$ through N_s corresponds to the soft layer which has magnetization, anisotropy, and exchange given by M_s, K_s, and A_s, respectively. The index $i=N_s+1$ through N represents the hard layer and is characterized by M_h, K_h, and A_h. The hard and soft layers are coupled at the interface by an exchange interaction A_{int}. The equilibrium spin configuration for a given field is determined by minimizing Eq. (4). For H parallel to the easy axis ($\theta_H=0$), the lowest energy configuration will be $\theta_i=0$ for all i. We are interested in the local-minimum configuration in which the hard layer is opposite to H ($\theta_i\sim\pi$ for $i=N_s+1$ to N) and the soft layer rotates with the applied field. To calculate this configuration we employ an iterative approach outlined by Camley.[17,18] We start with all spins at $\theta_i\sim\pi$ (for all $i=1$ to N) in a small positive applied field. A spin is then randomly chosen and rotated towards its lowest energy position. The new spin direction θ_i' is estimated by the following expression:

$$\tan(\theta_i')=\frac{A_{i,i-1}\sin(\theta_{i-1})+A_{i,i+1}\sin(\theta_{i+1})+d^2HM_i\sin(\theta_H)}{A_{i,i-1}\cos(\theta_{i-1})+A_{i,i+1}\cos(\theta_{i+1})+2d^2K_i\cos(\theta_i)+d^2HM_i\cos(\theta_H)}, \tag{5}$$

which is determined from the criterion that $dE/d\theta_i=0$. This procedure is repeated by randomly selecting spins and rotating them, via Eq. (5), until the system converges on a stable configuration. For a 200-spin system, this typically takes 10^5-10^6 iterations. The total longitudinal and transverse moments are calculated, the field is increased and the process repeated in order to calculate a hysteresis loop. Since the criterion $dE/d\theta_i=0$ is also valid for maxima as well as minima in the energy, some care is needed to avoid such solutions. One such solution can be obtained for $\theta_H=0$ and $\theta_i=\pi$ for all i, even if an applied field is sufficient to reverse the soft layer. To avoid this problem, we either perturb the system at each field to check the stability of the solution or we use a small but finite value of θ_H in our easy-axis calculations. Both methods give similar results. Since there is inevitably some misalignment between the field and the easy axis in an actual measurement, taking into account the misalignment angle in fact more closely simulates the real system.

Shown in Fig. 7(a) is the comparison of the calculated Sm-Co/Fe (200 Å) easy-axis loop to the 25-K data shown in Fig. 6. The parameters for the calculation are $A_h=1.2\times10^{-6}$ ergs/cm, $K_h=5\times10^7$ ergs/cm^3, $M_h=550$ emu/cm^3, $A_s=2.8\times10^{-6}$ergs/cm, $K_s=10^3$ ergs/cm^3, $M_s=1700$ emu/cm^3, $A_{int}=1.8\times10^{-6}$ ergs/cm, and $\theta_H=3°$. The values of K_h and M_h were estimated from magnetization measurements on the Sm-Co films. The value of A_{int} was set intermediate to exchange coupling of the hard and soft lay-

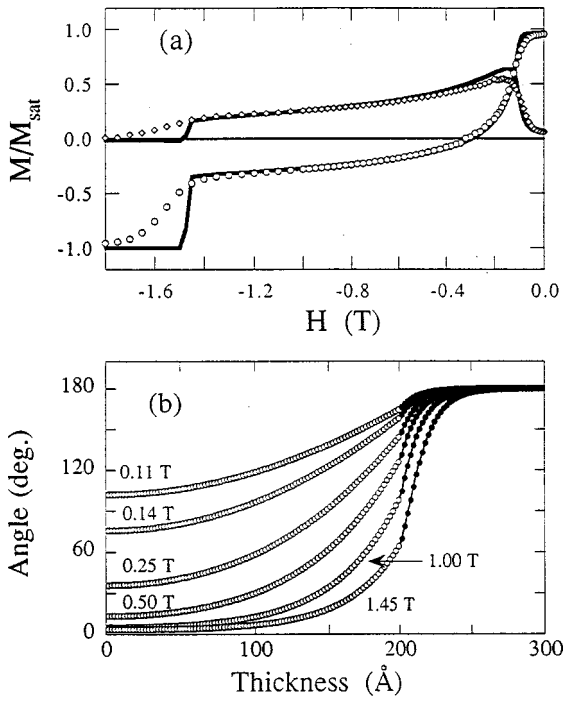

FIG. 7. (a) Low-temperature (25 K) demagnetization curves for the Sm-Co/Fe(200 Å) film shown in Fig. 6 compared to the model calculation (solid line) described in the text. The longitudinal and transverse components of the magnetization are given by the circles and triangles, respectively. (b) Representative spin configuration determined from the model calculation shown in (a). Open circles are Fe spins and filled circles are Sm-Co spins. The free Fe surface is located at zero and the Sm-Co/Fe interface is at 200 Å.

ers. The calculation reproduces the H_{ex} value, the field dependence of both the longitudinal and transverse magnetization, as well as the switching field of the Sm-Co layer at ~1.5 T. The irreversible switching of the hard layer is expected to be the least reliable parameter determined by this type of modeling and the close agreement in Fig. 7(a) is rather fortuitous. Shown in Fig. 7(b) is the spin configuration at various fields for the calculated magnetization in Fig. 7(a). The distribution of moments is consistent with the expectation that the Fe located away from the interface rotates more. For the configuration at $H=0.14$ T the average Fe angle is ~90° resulting in the maximum in the transverse moment with applied field. As the field increases, the turn angle of the Fe spins away from the interface increases and the surface layers align with the field. At $H=1.45$ T (just below the switching of the hard layer), the top ~120 Å of the Fe layer aligns with the field.

The hard layer is also significantly perturbed by the rotation of the Fe layers, in agreement with the calculations of Mibu *et al.*[5] As H increases, the interfacial Sm-Co spin is also increasingly rotated and a domain wall is slowly introduced into the hard layer. This domain wall, nucleated by the Fe layer, reverses the Sm-Co layer at a field well below that expected for an isolated Sm-Co film. In the calculation shown in Fig. 6, the Sm-Co layer reverses at $H=1.47$ T. If one sets $A_{int}=0$ to decouple the Fe and Sm-Co layers, the Sm-Co layer reverses at $H=15$ T. The reduction of the switching field of the hard layer was explained in Ref. 1. As the field increases, the domain wall in the soft layer is compressed and its energy increases. The wall energy in the soft layer γ_s, assuming no anisotropy, is expected to vary as $\sqrt{A_s M_s H}$. The energy of a domain wall in the hard layer is $\gamma_h = 4\sqrt{A_h K_h}$. As the field increases such that γ_s becomes greater than γ_h, the domain wall in the soft layer moves into, and switches, the hard layer. The field at which the hard layer switches should roughly scale as $A_h K_h / A_s M_s$ and is significantly lower than that for the isolated film. This also explains why the hard layer switches at a lower field in the Sm-Co/Co bilayers (see Fig. 6). Co has higher exchange and anisotropy constants than Fe, both of which increase γ_s and thus reduce the Sm-Co switching field.

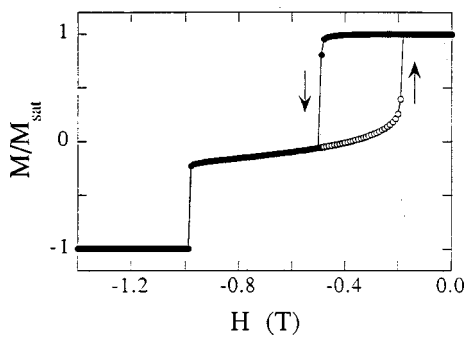

FIG. 8. Calculated demagnetization curves for the Sm-Co/Co(200 Å) film. The model parameters are described in the text.

We simulated the switching of the Sm-Co/Co(200 Å) bilayer. Shown in Fig. 8 are the calculated demagnetization curve and minor loop simulated for the 200-Å Co layer for parameters: $M_s=1400$ emu/cm^3, $A_s=4.0\times10^{-6}$ ergs/cm, and $K_s=3\times10^6$ ergs/cm^3. All the features of the measured data (Fig. 6) are reproduced in the calculations. In particular, the exchange field for the Co layer is large compared to that for Fe layers of similar thickness, the switching of the Co layer is hysteretic about H_{ex}, and the Sm-Co layer switches at a lower field than the Sm-Co/Fe films.

The reliability of the simulation can be checked by comparison to the room-temperature easy- and hard-axis data (both longitudinal and transverse. These comparisons are shown in Fig. 9. The parameters in the calculation are identical to those used in Fig. 7 with the exception that A_s is decreased by 8% to reflect the weakening with increased T. The same set of parameters is able to quantitatively reproduce the measured results, with the exception of the value of

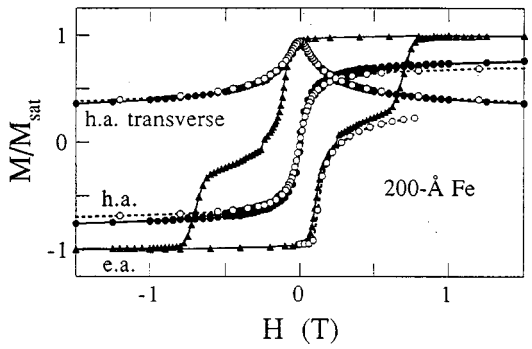

FIG. 9. Room-temperature hysteresis loops for the Sm-Co/Fe(200 Å) film shown in Fig. 2 (filled symbols) compared to the model calculation (open circles) described in the text.

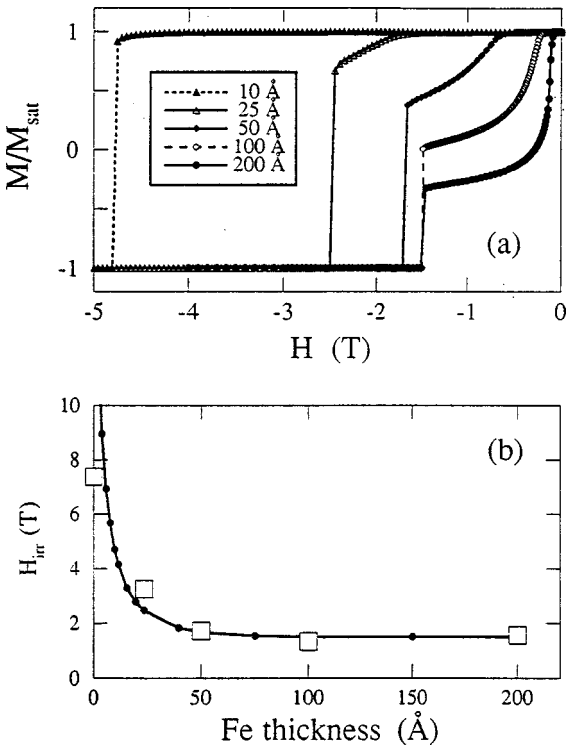

FIG. 10. (a) Calculated demagnetization curves for Sm-Co/Fe films with various Fe thicknesses. (b) Calculated irreversibility field for Sm-Co/Fe films as a function of Fe thickness compared to the measured values for the Sm-Co/Fe bilayer films measured at 25 K.

the room-temperature switching field of the hard layer. These parameters provide a reasonable description of the sample and provide added confidence in the assumption that the interfacial exchange is comparable with the exchange within the layer.

With these parameters we can simulate a series of hysteresis loops for different Fe layer thickness values. Shown in Fig. 10(a) are easy-axis demagnetization curves for different Fe layer thicknesses from 10 to 200 Å. The switching for the hard layer initially decreases dramatically with increasing Fe thickness. Even a 10-Å Fe layer reduces the calculated coercivity of the hard layer by a factor of 3. When the Fe-layer thickness become comparable to the width of a domain wall, the switching of the hard layer becomes independent of the Fe layer thickness. This is shown in Fig. 10(b) where the calculated Sm-Co switching fields are compared to those of the Sm-Co/Fe samples measured at 25 K. The general trend in the data is well reproduced by the simulations.

From the simulated hysteresis loops, we can extract the maximum energy product $(BH)_{\max}$ for the Fe/Sm-Co bilayer structure. Shown in Fig. 11 are the calculated $(BH)_{\max}$ curves plotted as a function of Fe layer thickness for different Sm-Co layer thicknesses. $(BH)_{\max}$ increases initially with increasing Fe thickness, peaks, and then decreases. The peak value of $(BH)_{\max}$ increases with decreasing Sm-Co thickness. Also shown as dashed curves is the ideal energy-product $(BH)_{\max}=(2\pi M_s)^2$. At low Fe thicknesses (less than the Block wall width in the hard layer), the Fe layer couples rigidly to the hard layer and the nucleation field H_N is greater than $2\pi M_s$. $(BH)_{\max}$ then increases as a result of the increased saturation magnetization, following the ideal curve.

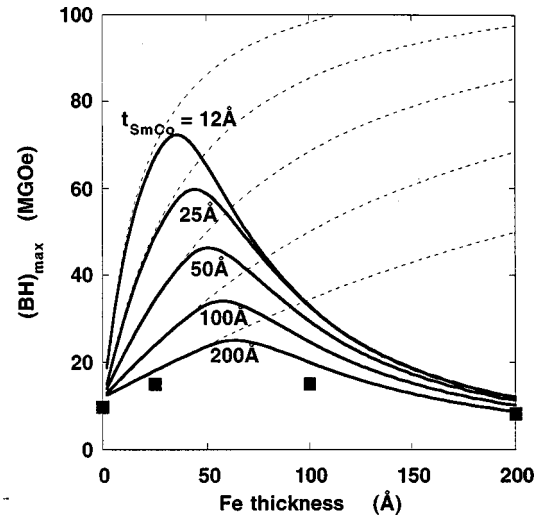

FIG. 11. Calculated maximum energy produce $(BH)_{\max}$ of Sm-Co/Fe bilayers with different layer thicknesses. The dashed curves are that of the ideal $(BH)_{\max}$. The square symbols are experimental $(BH)_{\max}$ values taken from the hysteresis loops shown in Fig. 2.

With increasing thickness, the Fe-layer magnetization reverses at lower fields, and $(BH)_{\max}$ is limited by the exchange bias field H_{ex}. The square symbols are the $(BH)_{\max}$ values taken from the hysteresis loops shown in Fig. 2. The agreement between the experimental data and model calculation is reasonably good. The calculation shows that for bilayers with suitably thin constituent layers, $(BH)_{\max}$ can even be greater than that of Nd-Fe-B, illustrating the importance of the exchange hardening mechanism.

The model does overestimate the switching fields for low Fe thickness as seen in Fig. 10(b). This results from an incomplete description for the Sm-Co layer. The present model does not include any other region to nucleate reversal besides the Fe layer and, thus, H_c for the isolated Sm-Co layer equals the anisotropy field (for $\theta_H=0$) which, of course, is never expected to be achieved in real films. However, as we have discussed previously, this does not affect the calculation of $(BH)_{\max}$.

V. CONCLUSION

We have presented the experimental results on strongly exchange-coupled Sm-Co(1100)/TM bilayer films. Because of the epitaxial growth, the magnetically hard Sm-Co layer has an in-plane uniaxial anisotropy field as large as 20 T. Such a large anisotropy field enables us to explore exchange-spring behavior in a new region where the soft-layer thicknesses are <20 nm. The moments in the soft layer near the interface are pinned by the hard layer and switch reversibly. The present results can be understood from the intrinsic parameters of the hard and soft layers, indicating that the interfacial coupling between the Sm-Co and the soft layer is comparable to the atomic exchange whether the soft layer is Fe or Co. It was suggested[1] that exchange coupling requires crystallographically coherent interfaces and therefore the hard and soft phases should emerge from a common matrix phase. The present results suggest that exchange coupling is a more general and robust phenomenon since Fe and Co have different crystal symmetries and both are strongly

coupled to the hard Co-Sm layer.

The fact that the experimental results and the simulation agree quantitatively permits the use of bilayers to model exchange-spring coupling in order to obtain detailed information about the magnetization reversal process and an estimate of the potential enhancement in the energy product that can be gained due to the exchange hardening principle. Thus, a simple bilayer system can provide guidance for the further development and optimization of high-performance permanent magnets.

ACKNOWLEDGMENT

Work at ANL was supported by the U.S. Department of Energy, BES-Materials Science, under Contract No. W-31-109-ENG-38.

*Present address: IBM Almaden Research Center, 650 Harry Rd., San Jose, CA 95120-6099.

[1] E. F. Kneller and R. Hawig, IEEE Trans. Magn. **27**, 3588 (1991).
[2] J. M. D. Coey, Solid State Commun. **102**, 101 (1997).
[3] R. Skomski, Phys. Rev. B **48**, 15 812 (1993).
[4] E. E. Fullerton, C. H. Sowers, J. P. Pearson, S. D. Bader, X. Z. Wu, and D. Lederman, Appl. Phys. Lett. **69**, 2438 (1996).
[5] K. Mibu, T. Nagahama, and T. Shinjo, J. Magn. Magn. Mater. **163**, 75 (1996).
[6] D. Givord, J. Betz, K. Mackay, J. C. Toussaint, J. Voiron, and S. Wüchner, J. Magn. Magn. Mater. **159**, 71 (1996).
[7] S. Wüchner, J. C. Toussaint, and J. Voiron, Phys. Rev. B **55**, 11 576 (1997).
[8] Y. Suzuki, R. B. van Dover, E. M. Gyorgy, J. M. Phillips, and R. J. Felder, Phys. Rev. B **53**, 14 016 (1996).
[9] I. A. Al-Omari and D. J. Sellmyer, Phys. Rev. B **52**, 3441 (1995).
[10] M. Shindo, M. Ishizone, H. Kato, T. Miyazaki, and A. Sakuma, J. Magn. Magn. Mater. **161**, 1 (1996).
[11] E. Goto, N. Hayashi, T. Miyashita, and K. Nakagawa, J. Appl. Phys. **36**, 2951 (1965).
[12] E. E. Fullerton, J. S. Jiang, C. Rehm, C. H. Sowers, S. D. Bader, J. B. Patel, and X. Z. Wu, Appl. Phys. Lett. **71**, 1579 (1997).
[13] M. Benaissa, K. M. Krishnan, E. E. Fullerton, and J. S. Jiang, IEEE Trans. Magn. **34**, 1204 (1998).
[14] K. H. J. Buschow, J. Less-Common Met. **33**, 311 (1973).
[15] K. J. Strnat and R. M. W. Strnat, J. Magn. Magn. Mater. **100**, 38 (1991).
[16] K. W. Damon and J. R. Eshbach, J. Phys. Chem. Solids **19**, 308 (1961).
[17] R. E. Camley, Phys. Rev. B **35**, 3608 (1987).
[18] R. E. Camley and D. R. Tilley, Phys. Rev. B **37**, 3413 (1988).